POLYOXOMETALATES RESEARCH ARTICLE

# Silver-modified polyniobotungstate for the visible light-induced simultaneous cleavage of C–C and C–N bonds

Shujun Li[1] ✉, Na Li[1], Gang Li[1], Yubin Ma[1], Mengyao Huang[1], Qingchun Xia[1], Qianyi Zhao[1] ✉, and Xuenian Chen[1,2] ✉

[1] *School of Chemistry and Chemical Engineering, Henan Key Laboratory of Boron Chemistry and Advanced Energy Materials, Key Laboratory of Green Chemical Media and Reactions, Ministry of Education, Henan Normal University, Xinxiang 453007, China*
[2] *Green Catalysis Center and College of Chemistry, Zhengzhou University, Zhengzhou 450001, China*

Cite This: *Polyoxometalates*, **2023**, *2*, 9140024 Read Online

**ABSTRACT:** Silver-modified polyniobotungstate based on Nb/W mixed-addendum polyoxometalate with formula $Ag_9[P_2W_{15}Nb_3O_{62}]\cdot 21H_2O$ (**Ag-Nb/W**) was synthesized and then characterized by various analytical and spectral techniques. **Ag-Nb/W** was proven to be an efficient photocatalyst for the oxidative ring opening of 2-phenylimidazo[1,2-*a*]pyridine via the simultaneous cleavage of C–C and C–N bonds. Under visible light (430–440 nm) and with oxygen as an oxidant at room temperature, **Ag-Nb/W** can catalyze the rapid transformation of various 2-phenylimidazo[1,2-*a*]pyridine derivatives to produce the corresponding oxidative ring-opening product N-(pyridin-2-yl) amides in good isolated yields ranging from 65% to 78%. As a heterogeneous photocatalyst, **Ag-Nb/W** showed excellent sustainability and recyclability in the recycling experiments. Infrared (IR) spectroscopy and X-ray diffraction (XRD) analysis indicated that **Ag-Nb/W** could retain its integrity after catalysis. A possible mechanism involving the singlet oxygen for the catalytic reaction was proposed.

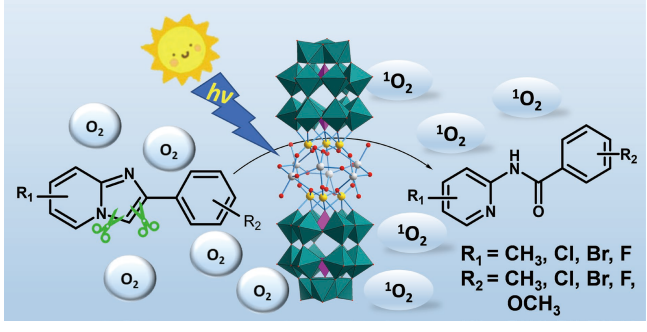


**KEYWORDS:** bond cleavage, polyniobotungstate, polyoxometalates, photocatalyst

## 1 Introduction

Polyoxometalates (POMs) are a large family of inorganic and anionic metal–oxygen clusters of early transition metal ions ($Mo^{6+}$, $W^{6+}$, $V^{5+}$, $Nb^{5+}$, and $Ta^{5+}$) [1–4]. Owing to their advantages of definite structures, adjustable elemental composition, and band gap, reversible multielectron processes, and high stability under redox conditions [5–9], POMs are promising candidates in the field of photocatalysis, including in the photocatalytic evolution of hydrogen [10–12], reduction of carbon dioxide [11–16], and degradation of organic pollutants [17–22]. In particular, POM photocatalysis has attracted sustained attention for organic chemical conversion [23–27]. Several POMs have shown potential in organic reactions, including aerobic oxidation [28–30], and some bond formation reactions, including the formation of C–C, C–N, C–O C–Si, C–P, and C–F bonds [31–39]. However, most POMs can only work using ultraviolet light. Thus, designing and synthesizing new visible light-promoted POM photocatalysts and exploring their potential in new organic reactions is of great significance. C–C and C–N bonds are the most widespread and fundamental bonds in organic compounds. Contrary to their highly developed formation, their selective cracking is difficult [40–42]. The selective catalytic cleavage of C–C bonds or C–N bonds for chemical transformations is an important topic in synthetic chemistry and has become one of the most attractive but challenging tasks [42, 43]. Over the past few decades, chemists have made great efforts and developed a variety of catalytic systems to separately cleave C–C or C–N bonds [44, 45]. However, the cleavage of C–C and C–N bonds in a single organic transformation has remained difficult. Only a few examples of the simultaneous cleavage of C–C and C–N bonds in one substrate molecule have been reported so far [34–48]. In addition, these reactions require harsh conditions, such as strong oxidant or initiator and high temperature (Schemes 1(a) and 1(b)) [47, 49]. Therefore, the rapid and simultaneous cleavage of C–C and C–N bonds under mild conditions with high regioselectivity is still a challenge.

Herein, we report a new silver-modified polyniobotungstate (**Ag-Nb/W**) obtained from the reaction between Nb/W mixed-

**Received:** November 22, 2022; **Revised:** January 6, 2023
**Accepted:** January 19, 2023

✉Address correspondence to Shujun Li, lisj@htu.edu.cn; Qianyi Zhao, qyzhao@htu.edu.cn; Xuenian Chen, xnchen@htu.edu.cn

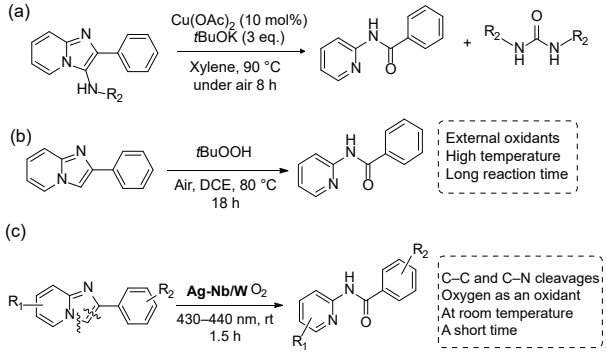


**Scheme 1** Ring-opening reactions via C–C and C–N bond cleavage under different conditions.

addendum POM $[P_2W_{15}Nb_3O_{62}]^{9-}$ and $Ag^+$ ion. **Ag-Nb/W** was proven to be a high-efficiency heterogeneous photocatalyst for the regioselective cleavage of C–C and C–N bonds in 2-phenylimidazo[1,2-*a*]pyridine under extremely mild conditions, namely, in an $O_2$ atmosphere at room temperature without using external oxidants and precious metals (Scheme 1(c)). To the best of our knowledge, this work is the first example of visible light-promoted simultaneous cleavage of C–C and C–N bonds catalyzed by a POM photocatalyst. This approach coincides with the social demand for "green chemistry" and "sustainable development".

## 2 Experimental

### 2.1 Materials and methods

The precursor $K_8H[P_2W_{15}(NbO_2)_3O_{59}]\cdot 12H_2O$ was synthesized as previously described [50]. All other reagents were obtained commercially and used without further purification. Fourier transform infrared (FT-IR) spectroscopy analysis in attenuated total refraction (ATR) mode was performed with a Perkin Elmer Spectrum 400 FT-IR/FT-FIR Spectrometer equipped with ATR objective lens in the range of 400–4000 $cm^{-1}$ at room temperature. Powder X-ray diffraction (PXRD) measurements were conducted on a Panalytical X'Pert3 Powder diffractometer with graphite monochromatized Cu K$\alpha$ radiation at 170 K. Thermal analyses was facilitated on a Netzsch 449C thermal analyzer. The sample was heated to 1000 °C with a heating rate of 5 °C/min under an $N_2$ atmosphere. X-ray photoelectron spectroscopy (XPS) was conducted on a Thermo Fisher Scientific ESCALAB250Xi X-ray photoelectron spectroscope. High-resolution mass spectra (HRMS) were recorded on a Bruker Mass spectrometer using electrospray ionization-time of flight (ESI-TOF). $^1H$ NMR spectra were recorded on a Bruker AVANCE III HD 600 MHz spectrometer.

### 2.2 Synthesis of Ag-Nb/W

$K_8H[P_2W_{15}(NbO_2)_3O_{59}]\cdot 12H_2O$ (0.20 g, 0.04 mmol) and $AgNO_3$ (0.35 g, 2.06 mmol) were dissolved in 20 mL of water. Nitric acid (1 M) was then added to adjust the pH of the reaction solution to 1.0–2.0, and the mixture was further stirred at 70 °C for 40 min. After cooling to room temperature, the reaction solution was filtered and allowed to evaporate. Bright yellow crystals were obtained within 1 week. Yield: 0.21 g (96.5% based on $K_8H[P_2W_{15}(NbO_2)_3O_{59}]\cdot 12H_2O$). Anal. Calcd. (%) for **Ag-Nb/W**: Ag 4.17, P 0.27, W 11.86, Nb 1.20; found Ag 4.02, P 0.26, W 11.44, Nb 1.16. IR (KBr disks): 1612 (w), 1079 (s), 943 (s), 908 (s), 709 (vs) $cm^{-1}$.

## 3 Results and discussion

### 3.1 Synthesis considerations

**Ag-Nb/W** was synthesized by the simple reaction of Nb/W mixed-addendum Dawson-type precursor $(K_8H[P_2W_{15}(NbO_2)_3O_{59}]\cdot 12H_2O)$ and $AgNO_3$ in a mild aqueous solution under conventional conditions. Details of the experiment are shown in the Electronic Supplementary Material (ESM). Owing to its low solubility in water, the yellow crystal product of **Ag-Nb/W** was obtained with a high yield close to 100% using a wide range of pH values (0.5–5.0) adjusted with nitric acid. However, single crystals suitable for single-crystal measurement can only be obtained from a solution of pH 1.0–2.0.

### 3.2 Structural descriptions

Single-crystal XRD analysis (Table S1 in the ESM) indicated that **Ag-Nb/W** crystallized in trigonal symmetry, $R\bar{3}$ space group. The asymmetrical unit of **Ag-Nb/W** contained one Dawson unit $[P_2W_{15}Nb_3O_{62}]^{9-}$ ($\{P_2W_{15}Nb_3\}$) and nine $Ag^+$. As shown in Fig. 1(a), each $\{P_2W_{15}Nb_3\}$ was surrounded and coordinated by 15 $Ag^+$. Three kinds of crystallographically distinct silver ions were observed: Ag1 and Ag3 are five-coordinated, and Ag2 is four-coordinated (Fig. 1(b)). Each Ag1 was coordinated to two terminal oxygen atoms bonded with Nb, $O_t$(Nb), and three coordination water molecules (Ow) with the Ag–O bond length of 2.30 and 2.67 Å and Ag–Ow distances in the range of 2.345–2.294 Å. Each Ag2 connected to two $\{P_2W_{15}Nb_3\}$ through two (Nb)$O_t$–Ag–$O_t$(W) bridges with Ag–O bond lengths of 2.355 and 2.345 Å and one water molecule with Ag–Ow distance of 2.22 Å. Each Ag3 was coordinated to one $O_t$(W), two $O_b$(W) with Ag–O distances of 2.57 and 2.58 Å, and two coordinated water molecules with Ag–Ow distances of 2.42 and 2.38 Å. Two $\{P_2W_{15}Nb_3\}$ were connected by six Ag1, forming a sandwich structure (Fig. 1(c) and Fig. S1 in the ESM). From another aspect, the six silver ions were coordinated by six $O_t$(Nb) atoms from $\{P_2W_{15}Nb_3\}$ and twelve coordinated water

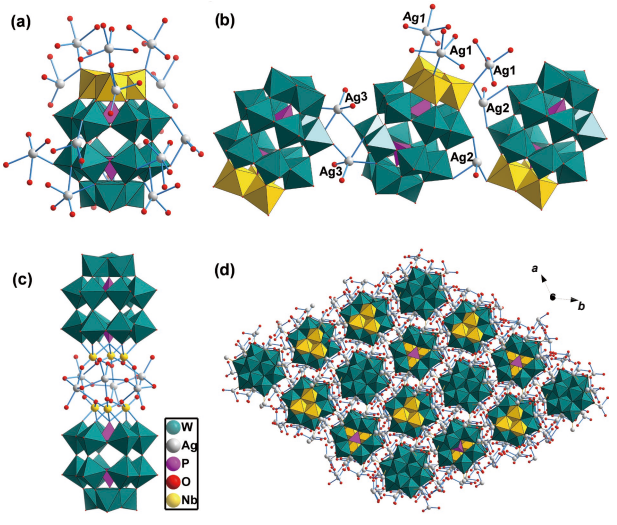


**Figure 1** (a) Combined polyhedral/ball-and-stick representation of the asymmetrical unit, (b) three adjacent $\{P_2W_{15}Nb_3\}$ connected by $Ag^+$ highlighting the coordination of three kinds of Ag ions, (c) the sandwich dimer connected by six $Ag^+$ and (d) the 3D network structure view along the *c* axis in Ag-Nb/W.

molecules, resulting in a rare silver-oxo cluster $\{Ag_6(H_2O)_{12}\}$. We believe that the coordination environment provided by the $\{P_2W_{15}Nb_3\}$ plays an important role in the formation of $\{Ag_6(H_2O)_{12}\}$ cluster in **Ag-Nb/W**. Furthermore, $\{Ag_6(H_2O)_{12}\}$ cluster bonded to another six Ag2 through Ag1–O30–Ag2 bridges, forming a $\{Ag_{12}(H_2O)_{18}\}$ cluster. In summary, each $\{P_2W_{15}Nb_3\}$ was connected to six surrounding $\{P_2W_{15}Nb_3\}$ by twelve Ag ions, forming a three-dimensional (3D) network structure (Fig. 1(d)).

### 3.3 Properties

In the ultraviolet–visible (UV–vis) diffuse reflection spectroscopy shown in Fig. 2(a), the yellow solid sample of **Ag-Nb/W** exhibited strong absorption in the visible region, indicating its potential application in photocatalysis. XPS was further employed to determine the chemical states of Ag and W in **Ag-Nb/W**. The peaks with binding energies at 374.6 and 368.6 eV corresponded to $Ag^+$ $3d_{3/2}$ and $Ag^+$ $3d_{5/2}$ states, respectively (Fig. 2(b)) [51]. These results were consistent with those from bond valence sum (BVS) analyses (Table S2 in the ESM). In addition, the W spectrum for **Ag-Nb/W** showed two binding energies at 38.0 and 35.9 eV, which represent the electrons of $W^{6+}$ states (Figs. S4 and S5 in the ESM) [52].

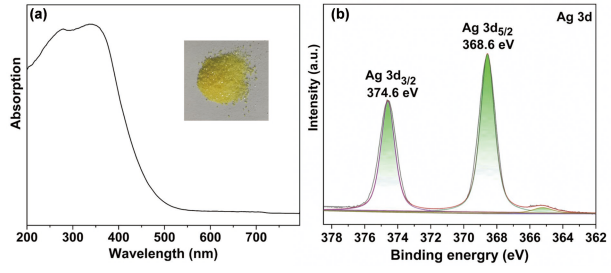


**Figure 2** (a) Diffuse reflectance spectrum of Ag-Nb/W (inset: photograph of the crystal sample). (b) XPS spectrum of Ag signals for Ag-Nb/W.

### 3.4 Photocatalytic performance

The strong adoption in the visible region exhibited by the yellow solid sample of **Ag-Nb/W** (Fig. 2(a)) prompted us to study its catalytic activity under visible light. We began our investigation with 2-phenylimidazo[1,2-*a*]pyridine (**1a**) as the model substrate to evaluate the catalyst and optimize the reaction conditions (Table 1). In our initial study, the reaction of 2-phenylimidazo[1,2-*a*]pyridine (0.2 mmol) in the presence of **Ag-Nb/W** (1.5 mol%) in ethanol generated the desired product N-(pyridine-2-yl)benzamide (**2a**) in 17% yield after 1.5 h irradiation under blue-LEDs (Table 1, entry 1). To optimize the reaction condition, we examined the effect of different solvents including ethanol, dichloromethane, toluene, acetone, n-hexane, tetrahydrofuran, methanol, and acetonitrile (entries 1–8) on the reaction and found that acetonitrile gave the highest yield of **2a** (78%, entry 8). We then studied the effect of the amount of catalyst and found that an increase in catalyst loading did not lead to a sustained increase in the reaction yield (entries 8–10). A good yield of 78% was obtained when the catalyst dosage was 1.5 mol% (entry 8), which was considered to be the optimized amount. Using the model substrate, we next examined the effect of the light source, namely, 10 W LED lamps with different wavelength bands including 390–400, 410–420, and 440–450 nm (entries 11–13) and a solar simulator (300 W Xe lamp) (entry 14). The results revealed that 430–440 nm was the best light source, leading to the desired product **2a** in good isolated yield (78%, entry 8) after 1.5 h. Finally, the optimized reaction conditions were established as follows: substrate (0.2 mmol), **Ag-Nb/W** (1.5 mol%), and solvent acetonitrile (2 mL) were irradiated by a blue LED light (10 W, 430–440 nm) and stirred under $O_2$ (1 atm) at room

**Table 1** Optimization of reaction conditions[a]

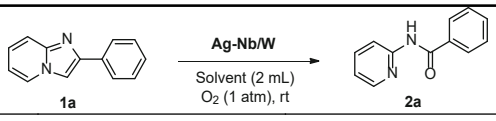


| Entry | Cat. | Light source (nm) | Solvent | Time (h) | Yield (%)[b] |
|---|---|---|---|---|---|
| 1 | 1.5 mol% **Ag-Nb/W** | 430–440 | Ethanol | 1.5 | 17 |
| 2 | 1.5 mol% **Ag-Nb/W** | 430–440 | Dichloromethane | 1.5 | 13 |
| 3 | 1.5 mol% **Ag-Nb/W** | 430–440 | Toluene | 1.5 | Trace |
| 4 | 1.5 mol% **Ag-Nb/W** | 430–440 | Acetone | 1.5 | 31 |
| 5 | 1.5 mol% **Ag-Nb/W** | 430–440 | n-Hexane | 1.5 | Trace |
| 6 | 1.5 mol% **Ag-Nb/W** | 430–440 | Tetrahydrofuran | 1.5 | 70 |
| 7 | 1.5 mol% **Ag-Nb/W** | 430–440 | Methanol | 1.5 | 15 |
| 8 | 1.5 mol% **Ag-Nb/W** | 430–440 | Acetonitrile | 1.5 | 78 |
| 9 | 1 mol% **Ag-Nb/W** | 430–440 | Acetonitrile | 1.5 | 70 |
| 10 | 2.0 mol% **Ag-Nb/W** | 430–440 | Acetonitrile | 1.5 | 74 |
| 11 | 1.5 mol% **Ag-Nb/W** | 390–400 | Acetonitrile | 1.5 | 69 |
| 12 | 1.5 mol% **Ag-Nb/W** | 410–420 | Acetonitrile | 1.5 | 76 |
| 13 | 1.5 mol% **Ag-Nb/W** | 440–450 | Acetonitrile | 1.5 | 67 |
| 14[c] | 1.5 mol% **Ag-Nb/W** | Sunlight | Acetonitrile | 1.5 | 55 |

[a] **1a** (0.2 mmol), **Ag-Nb/W** (1.5 mol%) and solvent (2 mL) under 10 W LED light for entries 1–8, 11–13, stirred at room temperature, and in $O_2$ for 1.5 h. [b] Isolated yield. [c] Irradiated by a 300 W Xe lamp (Perfectlight, Microsolar 300) with a cut-off filter of AM-1.5G.

temperature for 1.5 h.

Using the optimized reaction conditions (Table 1, entry 8), we investigated the substrate scope for the photocatalytic oxidation ring-opening reaction of 2-phenylimidazo[1,2-*a*]pyridine derivatives (Table 2). The results showed that **Ag-Nb/W** was efficient for various substrates with either electron withdrawing groups (–F, –Cl, –Br) or electron donating groups (–$CH_3$, –$OCH_3$). The corresponding oxidative ring-opening products N-(pyridine-2-yl)benzamide derivative (**2a**–**2v**) could be obtained in moderate-to-good isolated yields (65% to 78%).

When 2-phenylimidazo[1,2-*a*]pyridine bearing electron-donating groups (–$CH_3$, –$OCH_3$) and electron-withdrawing groups (–F, –Cl, –Br) were loaded on pyridyl, the corresponding oxidative ring-opening products were obtained in moderate-to-good yields (**2b**–**2l**). When the substituent was on the phenyl of 2-phenylimidazo[1,2-*a*]pyridine, the corresponding products were produced in 67%–75% yields (**2m**–**2s**). To our surprise, the design of the functional group in different positions of pyridyl or phenyl of 2-phenylimidazo[1,2-*a*]pyridine, including ortho-, meta-, and para- almost had no influence on the yields of the target products. Moderate-to-good yields (68%–75%) were obtained for electron withdrawing (–Cl) and electron donating groups (–$CH_3$) at different positions of the pyridyl ring such as ortho, meta, and para positions (**2f**–**2h**, **2b**–**2d**). When the substituents were on the benzene ring, the corresponding products were also obtained in good yields (**2m**–**2s**). The yields of the corresponding ring-opened products were not affected in any way when the substituents simultaneously replaced H on the pyridine ring and any position on the benzene ring (**2t**–**2v**).

We performed a set of control experiments to further understand the reaction mechanism (Table 3). The results indicated that the catalytic activities of the precursors {$P_2W_{15}Nb_3$} and $AgNO_3$ were far lower than that of **Ag-Nb/W** (entries 1 and 2). The catalytic activity of the mixture {$P_2W_{15}Nb_3$}+$AgNO_3$ (entry 3) was better than that of any single constituent, indicating a synergy between them. Without any catalyst, only 21% yield of **2a** (entry 4) could be obtained. In the absence of light, **2a** was not produced in the reaction, indicating that light is necessary for the experimental process (entry 5). When oxygen was replaced by air or nitrogen, only minimal or none **2a** can be obtained (entries 6 and 7), indicating that oxygen is necessary for the reaction.

We examined the ring-opening reaction of 2-phenylimidazo[1,2-*a*]pyridine by adding free radical scavenger 2,2,6,6-tetramethylpiperidinyl-oxy and superoxide radical scavenger 4-benzoquinone under standard experimental conditions (Table 3, entries 8 and 9). The results showed that 75% and 73% of **2a** were isolated, implying the reaction is not carried out by a free radical mechanism. When α-terpinene was introduced into the reaction, the yield of **2a** was inhibited and almost no ring-opening products were obtained (entry 10). The oxidation product of terpinene was detected by ESI-HRMS (Scheme 2 and Fig. S12 in the ESM). These results indicated that the reaction is carried out by a singlet oxygen process.

Basing on our experimental results and a previous report [45], we proposed a reaction mechanism for the oxidative ring opening of 2-phenylimidazo[1,2-*a*]pyridine (**1a**) as shown in Scheme 3. First, the reaction starts from the transformation of ground state **Ag-Nb/W** to excited state **Ag-Nb/W**$^*$ under the irradiation of visible light. **Ag-Nb/W**$^*$ then reacts with ground state triplet oxygen ($^3O_2$) by energy transfer to obtain singlet oxygen ($^1O_2$). The reaction of **1a** with $^1O_2$ generates an unstable four-membered peroxide intermediate **A**, which is possibly converted to ring-opening product **B**. Subsequently, the C–H bond of the aldehyde intermediate (**B**) breaks, and the singlet oxygen is inserted to form peroxy acid (**C**). **C** reacts with one molecule **B** to form intermediate

**Table 2** Substrate scopes[a]

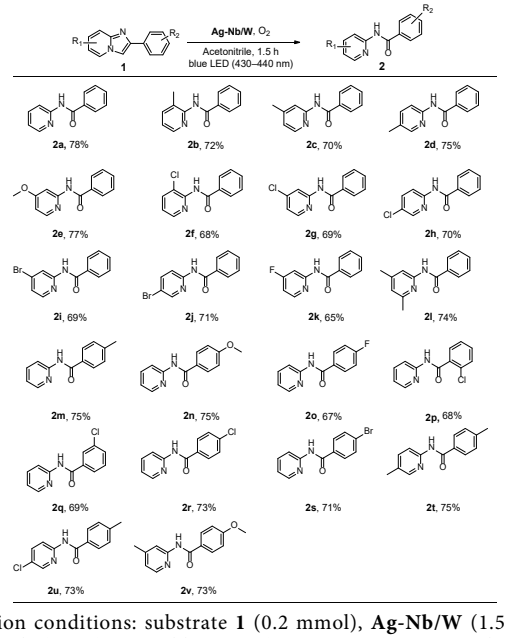


[a] Reaction conditions: substrate **1** (0.2 mmol), **Ag-Nb/W** (1.5 mol%), acetonitrile (2 mL), 10 W blue LED (430–440 nm), using $O_2$ balloon at room temperature for 1.5 h. Isolated yields were given.

**Table 3** Control experiments[a]

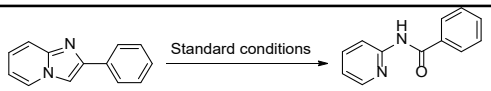


| Entry | Varied condition | Yield (%)[b] |
|---|---|---|
| 1 | $P_2W_{15}Nb_3$ | 31 |
| 2 | $AgNO_3$ | 29 |
| 3 | $P_2W_{15}Nb_3$ + $AgNO_3$ | 37 |
| 4[c] | — | 21 |
| 5[d] | 1.5 mol% **Ag-Nb/W** | — |
| 6 | Air instead of $O_2$ | 21 |
| 7 | $N_2$ instead of $O_2$ | none |
| 8 | TEMPO | 75 |
| 9 | BQ | 73 |
| 10 | α-Terpinene | — |

[a] All reactions were performed using **1a** (0.2 mmol), **Ag-Nb/W** (1.5 mol%) and acetonitrile (2 mL) under 10 W LED (430–440 nm), stirred at room temperature in $O_2$ for 1.5 h. [b]Isolated yield. [c] Without any catalyst. [d] Dark.

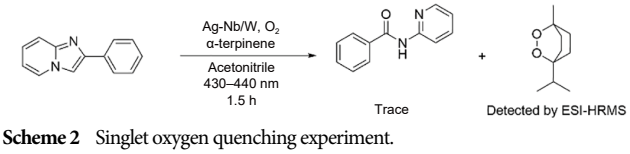


**Scheme 2** Singlet oxygen quenching experiment.

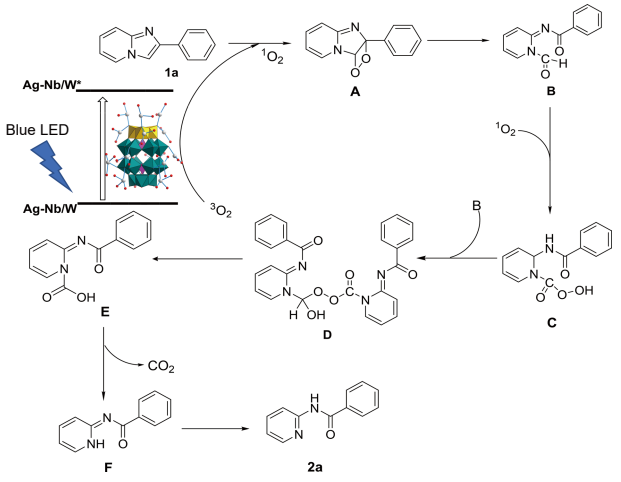


**Scheme 3** Proposed reaction mechanism.

**D** and then decomposes to form carboxylic acid compound **E**. Finally, intermediate **E** decarboxylates to release $CO_2$, and then aromatic cyclizes to produce the active species **F**, which could be isomerized to form the ring-opening product **2a**. Intermediates **A**, **B**, **C**, and **F** were detected by HRMS (Figs. S8–S11 in the ESM).

We also evaluated the stability and reusability of **Ag-Nb/W**. After the catalytic reaction, **Ag-Nb/W** was isolated by centrifugation, washed with ethanol, air-dried at room temperature for 24 h, and reused for the next round. No reduction in yield was observed after the 8th run (Fig. 3(a)). The PXRD patterns and FT-IR spectrum of the recovered **Ag-Nb/W** remained unchanged (Fig. 3(b) and Fig. S3 in the ESM), indicating that **Ag-Nb/W** is stable and the crystal lattice is mainly retained after catalysis. After **Ag-Nb/W** was removed from the reaction system during the reaction, no increase in **2a** yield was observed (Fig. S6 in the ESM), implying the heterogeneous nature of the catalyst system.

## 4 Conclusions

A purely inorganic photocatalyst **Ag-Nb/W** based on Nb/W mixed-addendum POM and Ag ions was synthesized at a high yield under simple and mild reaction conditions. **Ag-Nb/W** can efficiently catalyze the oxidative ring openings of 2-phenylimidazo[1,2-*a*]pyridine via the simultaneous cleavage of C–C and C–N bonds under visible light using $O_2$ as an oxidant. Mechanistic investigations suggested that a singlet oxygen process is the underlying mechanism of the catalytic reaction. As a heterogeneous photocatalyst, **Ag-Nb/W** shows good stability and reusability and could be reused eight times without any reduction in its catalytic activity. This work provides a feasible method for designing new visible light-induced polyoxometalate photocatalysts to be used in organic reactions involving the cleavage of C–C and C–N bonds.

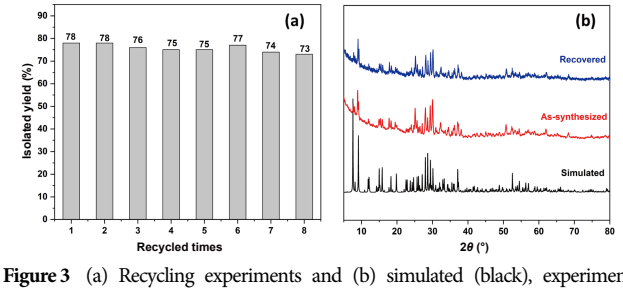


**Figure 3** (a) Recycling experiments and (b) simulated (black), experimental (red) and recovered (blue) PXRD patterns of Ag-Nb/W.

**Electronic Supplementary Material**: Supplementary material (crystallographic data, TG curve, IR spectra, XPS spectra, and NMR spectra for all products) is available in the online version of this article at https://doi.org/10.26599/POM.2023.9140024.

## Acknowledgements

This work was supported by the National Natural Science Foundation of China (Nos. 22171073 and U1804253) and the Program for Science & Technology Innovation Talents in Universities of Henan Province (No. 23HASTIT005).

## Declaration of competing interest

The authors have no competing interests to declare that are relevant to the content of this article.

## Author contribution statement

The manuscript was written through contributions of all authors.

## References

[1] Pope, M. T.; Müller, A. Polyoxometalate chemistry: An old field with new dimensions in several disciplines. *Angew. Chem., Int. Ed.* **1991**, *30*, 34–48.

[2] Long, D. L.; Tsunashima, R.; Cronin, L. Polyoxometalates: Building blocks for functional nanoscale systems. *Angew. Chem., Int. Ed.* **2010**, *49*, 1736–1758.

[3] Zheng, S. T.; Yang, G. Y. Recent advances in paramagnetic-TM-substituted polyoxometalates (TM = Mn, Fe, Co, Ni, Cu). *Chem. Soc. Rev.* **2012**, *41*, 7623–7646.

[4] Liu, J. C.; Wang, J. F.; Han, Q.; Shangguan, P.; Liu, L. L.; Chen, L. J.; Zhao, J. W.; Streb, C.; Song, Y. F. Multicomponent self-assembly of a giant heterometallic polyoxotungstate supercluster with antitumor activity. *Angew. Chem., Int. Ed.* **2021**, *60*, 11153–11157.

[5] Yamase, T. Photo- and electrochromism of polyoxometalates and related materials. *Chem. Rev.* **1998**, *98*, 307–326.

[6] Wang, S. S.; Yang, G. Y. Recent advances in polyoxometalate-catalyzed reactions. *Chem. Rev.* **2015**, *115*, 4893–4962.

[7] Yang, G. P.; Li, K.; Hu, C. W. Recent advances in uranium-containing polyoxometalates. *Inorg. Chem. Front.* **2022**, *9*, 5408.

[8] López, X.; Carbó, J. J.; Bo, C.; Poblet, J. M. Structure, properties and reactivity of polyoxometalates: A theoretical perspective. *Chem. Soc. Rev.* **2012**, *41*, 7537–7571.

[9] Liu, Y.; Tang, C. S.; Cheng, M.; Chen, M.; Chen, S.; Lei, L.; Chen, Y. S.; Yi, H.; Fu, Y. K.; Li, L. Polyoxometalate@metal-organic framework composites as effective photocatalysts. *ACS Catal.* **2021**, *11*, 13374–13396.

[10] Zhang, M.; Li, H. J.; Zhang, J. H.; Lv, H. J.; Yang, G. Y. Research advances of light-driven hydrogen evolution using polyoxometalate-based catalysts. *Chin. J. Catal.* **2021**, *42*, 855–871.

[11] Li, S. J.; Liu, S. M.; Liu, S. X.; Liu, Y. W.; Tang, Q.; Shi, Z.; Ouyang, S. X.; Ye, J. H. {$Ta_{12}$}/{$Ta_{16}$} cluster-containing polytantalotungstates with remarkable photocatalytic $H_2$ evolution activity. *J. Am. Chem. Soc.* **2012**, *134*, 19716–19721.

[12] Zhang, M.; Xin, X.; Feng, Y. Q.; Zhang, J. H.; Lv, H. J.; Yang, G. Y. Coupling Ni-substituted polyoxometalate catalysts with water-soluble CdSe quantum dots for ultraefficient photogeneration of hydrogen under visible light. *Appl. Catal. B Environ.* **2022**, *303*, 120893.

[13] Li, X. X.; Zhang, L.; Liu, J.; Yuan, L.; Wang, T.; Wang, J. Y.; Dong, L. Z.; Huang, K.; Lan, Y. Q. Design of crystalline reduction-oxidation cluster-based catalysts for artificial photosynthesis. *JACS Au* **2021**, *1*,

1288–1295.
[14] Li, X. X.; Zhang, L.; Yuan, L.; Wang, T.; Dong, L. Z.; Huang, K.; Liu, J.; Lan, Y. Q. Constructing crystalline redox catalyst to achieve efficient $CO_2$ photoreduction reaction in water vapor. *Chem. Eng. J.* **2022**, *442*, 136157.
[15] Yao, S. J.; Li, N.; Liu, J.; Dong, L. Z.; Liu, J. J.; Xin, Z. F.; Li, D. S.; Li, S. L.; Lan, Y. Q. Ferrocene-functionalized crystalline biomimetic catalysts for efficient $CO_2$ photoreduction. *Inorg. Chem.* **2022**, *61*, 2167–2173.
[16] Gu, J.; Chen, W.; Shan, G. G.; Li, G.; Sun, C.; Wang, X. L.; Su, Z. The roles of polyoxometalates in photocatalytic reduction of carbon dioxide. *Mater. Today Energy* **2021**, *21*, 100760.
[17] Lan, J.; Wang, Y.; Huang, B.; Xiao, Z. C.; Wu, P. F. Application of polyoxometalates in photocatalytic degradation of organic pollutants. *Nanoscale Adv.* **2021**, *3*, 4646–4658.
[18] Lai, S. Y.; Ng, K. H.; Cheng, C. K.; Nur, H.; Nurhadi, M.; Arumugam, M. Photocatalytic remediation of organic waste over keggin-based polyoxometalate materials: A review. *Chemosphere* **2021**, *263*, 128244.
[19] Li, H. L.; Zhang, M.; Lian, C.; Lang, Z. L.; Lv, H. J.; Yang, G. Y. Ring-shaped polyoxometalate built by $\{Mn_4PW_9\}$ and $PO_4$ units for efficient visible-light-driven hydrogen evolution. *CCS Chem.* **2021**, *3*, 2095–2103.
[20] Xia, Z. N.; Wang, L. B.; Zhang, Q.; Li, F. Y.; Xu, L. Fast degradation of phenol over porphyrin-polyoxometalate composite photocatalysts under visible light. *Polyoxometalates* **2022**, *1*, 9140001.
[21] Zang, D. J.; Wang, H. Q. Polyoxometalate-based nanostructures for electrocatalytic and photocatalytic $CO_2$ reduction. *Polyoxometalates* **2022**, *1*, 9140006.
[22] Yang, L.; Zhang, Z.; Zhang, C. N.; Li, S.; Liu, G. C.; Wang, X. L. An excellent multifunctional photocatalyst with a polyoxometalate-viologen framework for CEES oxidation, Cr(VI) reduction and dye decolorization under different light regimes. *Inorg. Chem. Front.* **2022**, *9*, 4824–4833.
[23] Qin, K. J.; Zang, D. J.; Wei, Y. G. Polyoxometalates based compounds for green synthesis of aldehydes and ketones. *Chin. Chem. Lett.*, in press, https://doi.org/10.1016/j.cclet.2022.107999.
[24] Hiskia, A.; Mylonas, A.; Papaconstantinou, E. Comparison of the photoredox properties of polyoxometallates and semiconducting particles. *Chem. Soc. Rev.* **2001**, *30*, 62–69.
[25] Suzuki, K.; Mizuno, N.; Yamaguchi, K. Polyoxometalate photocatalysis for liquid-phase selective organic functional group transformations. *ACS Catal.* **2018**, *8*, 10809–10825.
[26] Streb, C.; Kastner, K.; Tucher, J. Polyoxometalates in photocatalysis. *Phys. Sci. Rev.* **2019**, *4*, 20170177.
[27] Li, H. F.; Yang, M. N.; Yuan, Z. L.; Sun, Y. H.; Ma, P. T.; Niu, J. Y.; Wang, J. P. Construction of one $Ru_2W_{12}$-cluster and six lacunary Keggin tungstoarsenate leading to the larger Ru-containing polyoxometalate photocatalyst. *Chin. Chem. Lett.* **2022**, *33*, 4664–4668.
[28] Ravelli, D.; Protti, S.; Fagnoni, M. Decatungstate anion for photocatalyzed "window ledge" reactions. *Acc. Chem. Res.* **2016**, *49*, 2232–2242.
[29] Lykakis, I. N.; Tanielian, C.; Seghrouchni, R.; Orfanopoulos, M. Mechanism of decatungstate photocatalyzed oxygenation of aromatic alcohols: Part II. Kinetic isotope effects studies. *J. Mol. Catal. A Chem.* **2007**, *262*, 176–184.
[30] Liu, Y.-F.; Hu, C.-W.; Yang, G.-P. Recent advances in polyoxometalates acid-catalyzed organic reactions. *Chin. Chem. Lett.*, in press, https://doi.org/10.1016/j.cclet.2022.108097.
[31] Huang, X. Q.; Liu, S.; Liu, G.; Tao, Y. W.; Wang, C. R.; Zhang, Y. L.; Li, Z.; Wang, H. W.; Zhou, Z.; Shen, G. D. et al. An unprecedented 2-fold interpenetrated *lvt* open framework built from $Zn_6$ ring seamed trivacant polyoxotungstates used for photocatalytic synthesis of pyridine derivatives. *Appl. Catal. B Environ.* **2023**, *323*, 122134.
[32] Gu, Y. Q.; Li, Q.; Zang, D. J.; Huang, Y. C.; Yu, H.; Wei, Y. G. Light-induced efficient hydroxylation of benzene to phenol by quinolinium and polyoxovanadate-based supramolecular catalysts. *Angew. Chem., Int. Ed.* **2021**, *60*, 13310–13316.
[33] Ma, Y. B.; Gao, F.; Xiao, W. R.; Li, N.; Li, S. J.; Yu, B.; Chen, X. N. Two transition-metal-modified Nb/W mixed-addendum polyoxometalates for visible-light-mediated aerobic benzylic C-H oxidations. *Chin. Chem. Lett.* **2022**, *33*, 4395–4399.
[34] Ryu, I.; Tani, A.; Fukuyama, T.; Ravelli, D.; Montanaro, S.; Fagnoni, M. Efficient C-H/C-N and C-H/C-CO-N conversion via decatungstate-photoinduced alkylation of diisopropyl azodicarboxylate. *Org. Lett.* **2013**, *15*, 2554–2557.
[35] Li, S. J.; Li, G.; Ji, P. P.; Zhang, J. W.; Liu, S. X.; Zhang, J.; Chen, X. N. A giant Mo/Ta/W ternary mixed-addenda polyoxometalate with efficient photocatalytic activity for primary amine coupling. *ACS Appl. Mater. Interfaces* **2019**, *11*, 43287–43293.
[36] Sarver , P. J.; Bacauanu , V.; Schultz , D. M.; DiRocco, D. A.; Lam, Y. H.; Sherer, E. C.; MacMillan, D. W. C. The merger of decatungstate and copper catalysis to enable aliphatic C($sp^3$)-H trifluoromethylation. *Nat. Chem.* **2020**, *12*, 459–467.
[37] Jiao, J. C.; Yan, X. M.; Xing, S. Z.; Zhang, T.; Han, Q. X. Design of a polyoxometalate-based metal-organic framework for photocatalytic C($sp^3$)-H oxidation of toluene. *Inorg. Chem.* **2022**, *61*, 2421–2427.
[38] Zhao, W. Z.; Zeng, X. H.; Huang, L.; Qiu, S. Q.; Xie, J. Y.; Yu, H.; Wei, Y. G. Oxidative dehydrogenation of hydrazines and diarylamines using a polyoxomolybdate-based iron catalyst. *Chem. Commun.* **2021**, *57*, 7677–7680.
[39] Nodwell, M. B.; Yang, H.; Colović, M.; Yuan, Z. L.; Merkens, H.; Martin, R. E.; Bénard, F.; Schaffer, P.; Britton, R. $^{18}$F-fluorination of unactivated C-H bonds in branched aliphatic amino acids: Direct synthesis of oncological positron emission tomography imaging agents. *J. Am. Chem. Soc.* **2017**, *139*, 3595–3598.
[40] Chen, F.; Wang, T.; Jiao, N. Recent advances in transition-metal-catalyzed functionalization of unstrained carbon-carbon bonds. *Chem. Rev.* **2014**, *114*, 8613–8661.
[41] Souillart, L.; Cramer, N. Catalytic C-C bond activations via oxidative addition to transition metals. *Chem. Rev.* **2015**, *115*, 9410–9464.
[42] Yang, G. P.; Li, K.; Liu, W.; Zeng, K.; Liu, Y. F. Copper-catalyzed aerobic oxidative C-C bond cleavage of simple ketones for the synthesis of amides. *Org. Biomol. Chem.* **2020**, *18*, 6958–6964.
[43] Chen, W. M.; Xie, X.; Zhang, J.; Qu, J.; Luo, C.; Lai, Y. Z.; Jiang, F.; Yu, H.; Wei, Y. G. Oxidative carbon-carbon bond cleavage of 1,2-diols to carboxylic acids/ketones by an inorganic-ligand supported iron catalyst. *Green Chem.* **2021**, *23*, 9140–9146.
[44] Tang, C. H.; Jiao, N. Copper-catalyzed aerobic oxidative C-C bond cleavage for C-N bond formation: From ketones to amides. *Angew. Chem., Int. Ed.* **2014**, *53*, 6528–6532.
[45] Ritu; Sharma, C.; Kumar, S.; Jain, N. Singlet oxygen mediated dual C-C and C-N bond cleavage in visible light. *Org. Biomol. Chem.* **2020**, *18*, 2921–2928.
[46] Dreis, A. M.; Douglas, C. J. Catalytic carbon-carbon $\sigma$ bond activation: An intramolecular carbo-acylation reaction with acylquinolines. *J. Am. Chem. Soc.* **2009**, *131*, 412–413.
[47] Yan, K. L.; Yang, D. S.; Wei, W.; Li, G. Q.; Sun, M. Y.; Zhang, Q. Y.; Tian, L. J.; Wang, H. Metal-free TBHP-mediated oxidative ring openings of 2-arylimidazopyridines *via* regioselective cleavage of C-C and C-N bonds. *RSC Adv.* **2015**, *5*, 100102–100105.
[48] Chen, Z. W.; Wen, X. W.; Qian, Y. P.; Liang, P.; Liu, B. T.; Ye, M. Ce(III)-catalyzed highly efficient synthesis of pyridyl benzamides from aminopyridines and nitroolefins without external oxidants. *Org. Biomol. Chem.* **2018**, *16*, 1247–1251.
[49] Xu, F. Z.; Wang, Y. Y.; Xun, X. W.; Huang, Y.; Jin, Z. C.; Song, B. A.; Wu, J. Diverse oxidative C($sp^2$)-N bond cleavages of aromatic fused imidazoles for synthesis of α-ketoamides and *N*-(pyridin-2-

yl)arylamides. *J. Org. Chem.* **2019**, *84*, 8411–8422.
[50] Gong, J.; Chen, Y. G.; Qu, L. Y.; Liu, Q. Preparation and characterization of new peroxyniobium-containing phosphotungstates with Dawson structures. *Polyhedron* **1996**, *15*, 2273–2277.
[51] Romand, M.; Roubin, M.; Deloume, J. P. ESCA studies of some copper and silver selenides. *J. Electron Spectrosc. Relat. Phenom.* **1978**, *13*, 229–242.
[52] Kuznetsova, A. A.; Volchek, V. V.; Yanshole, V. V.; Fedorenko, A. D.; Kompankov, N. B.; Kokovkin, V. V.; Gushchin, A. L.; Abramov, P. A.; Sokolov, M. N. Coordination of Pt(IV) by $\{P_8W_{48}\}$ macrocyclic inorganic cavitand: Structural, solution, and electrochemical studies. *Inorg. Chem.* **2022**, *61*, 14560–14567.

**Shujun Li** received his B.S. degree from Hubei Normal University in 2008 and obtained his Ph.D. degree from Northeast Normal University in 2013 with the supervision of Prof. Shuxia Liu. He worked as a visiting scholar at University of Ulm, Germany, in 2021–2022. Now, he is an associate professor at Henan Normal University. His current research interest is concentrated on mixed-metal POMs and organoboron-functionalized POMs.

**Na Li** was born in 1996 in Hebei Provence. She is currently pursuing her master degree in the School of Chemistry and Chemical Engineering from Henan Normal University. Her current research focus is on POM photocatalysis for organic chemical conversion.

**Gang Li** was born in 1992 in Henan Provence. He received his B.S. and M.S. degrees from Henan Normal University in 2017 and 2020. He is currently a Ph.D. candidate in Harbin University of Science and Technology.

**Yubin Ma** was born in 1995 in Henan Provence. He obtained his master degree from the School of Chemistry and Chemical Engineering in Henan Normal University in 2022.

**Mengyao Huang** was born in 2000 in Henan Provence. She is currently pursuing her master degree in the School of Chemistry and Chemical Engineering from Henan Normal University. Her current research focus on the design and synthesis of POMs-based photocatalysts.

**Qingchun Xia** received his Ph.D. in chemistry from Shanghai Jiao Tong University in 2017. Currently he is a faculty in Henan Normal University. His research focuses on the synthesis and application of the boron-based metal-organic frameworks.

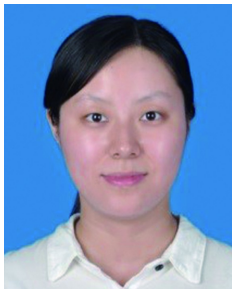

**Qianyi Zhao** received her Ph.D. in organic chemistry from Xiamen University in 2012. Currently she is a faculty in Henan Normal University. Her research focuses on the fundamental synthesis and application of boron-based compounds.

**Xuenian Chen** received his B.S. and M.S. degrees from Lanzhou University, and his Ph.D. from Lanzhou Institute of Chemical Physics, Chinese Academy of Sciences. He did postdoctoral work with Prof. S. G. Shore and was then appointed Research Scientist at the Department of Chemistry and Biochemistry and the Department of Materials Science and Engineering at The Ohio State University. He is currently a Distinguished Professor in the College of Chemistry at Zhengzhou University. His research interests are in boron chemistry, organometallics, catalysis, and materials science